THE JOURNAL OF PHYSICAL CHEMISTRY B

Article

pubs.acs.org/JPCB

Insights into the Transport of Aqueous Quaternary Ammonium Cations: A Combined Experimental and Computational Study

Himanshu N. Sarode,[†,⊥] Gerrick E. Lindberg,[‡,⊥] Yuan Yang,[§] Lisa E. Felberg,[‡] Gregory A. Voth,*[,‡] and Andrew M. Herring*[,†]

[†]Department of Chemical and Biological Engineering and [§]Department of Chemistry and Geochemistry, Colorado School of Mines, Golden, Colorado 80401, United States

[‡]Department of Chemistry, James Franck Institute, Institute for Biophysical Dynamics, and Computation Institute, University of Chicago, Chicago, Illinois 60637, United States

Supporting Information

ABSTRACT: This study focuses on understanding the relative effects of ammonium substituent groups (we primarily consider tetramethylammonium, benzyltrimethylammonium, and tetraethylammonium cations) and anion species (OH^-, HCO_3^-, CO_3^{2-}, Cl^-, and F^-) on ion transport by combining experimental and computational approaches. We characterize transport experimentally using ionic conductivity and self-diffusion coefficients measured from NMR. These experimental results are interpreted using simulation methods to describe the transport of these cations and anions considering the effects of the counterion. It is particularly noteworthy that we directly probe cation and anion diffusion with pulsed gradient stimulated echo NMR and molecular dynamics simulations, corroborating these methods and providing a direct link between atomic-resolution simulations and macroscale experiments. By pairing diffusion measurements and simulations with residence times, we were able to understand the interplay between short-time and long-time dynamics with ionic conductivity. With experiment, we determined that solutions of benzyltrimethylammonium hydroxide have the highest ionic conductivity (0.26 S/cm at 65 °C), which appears to be due to differences for the ions in long-time diffusion and short-time water caging. We also examined the effect of CO_2 on ionic conductivity in ammonium hydroxide solutions. CO_2 readily reacts with OH^- to form HCO^-_3 and is found to lower the solution ionic conductivity by almost 50%.

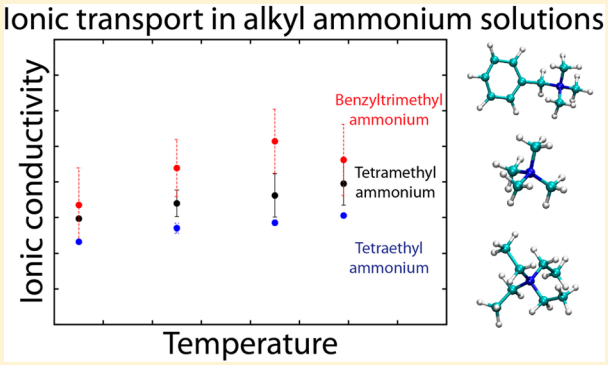

1. INTRODUCTION

Quaternary ammonium cations (R_4N^+) are important in medicine,[1,2] batteries,[3] alkaline anion exchange membranes (AEMs),[4,5] ionic liquids,[6] polymerizable surfactants,[7] and phase-transfer catalysts.[8] The quaternary ammonium cations with short alkyl side chains are highly soluble in water, but lengthening the alkyl chain or changing the composition can increase the hydrophobicity. There is a lack of fundamental understanding of various technologically important quaternary ammonium cations in nondilute aqueous solutions with anions such as hydroxide or carbonate, which is relevant to emerging electrochemical AEM applications such as fuel cells and electrolyzers.[9,10] Considerable experimental and theoretical efforts have been devoted to studying the structure, thermodynamics, and properties of these cations with halide counterions.[11−14] Similar studies have been performed with small acids like sulfonic acid, phosphonic acid, and trifluoromethanesulfonic acid, which are important for proton exchange membranes used in fuel cells.[15−17] The hydrophilic nature of the cations in the presence of Cl^- and Br^- was studied by Koga and co-workers,[18] showing the proclivity of tetramethyl ammonium (TMA) and tetraethyl ammonium (TEA) toward water. The literature is conflicting in that there is evidence for clathrate-like hydration shells around R_4N^+,[19] but other work claims that H_2O near ammonium is no different from pure H_2O.[20−22]

In addition to the properties of these ammonium ions in water, it is also interesting to consider the effect of these cations on anions in solution. Notably, AEM fuel cells commonly rely on quaternary ammonium[4,23−25] and quaternary phosphonium[26−28] based electrolyte membranes to facilitate hydroxide transport from the cathode to the anode.[5] When evaluating materials for AEM fuel cells, it is common to substitute less caustic anions for hydroxide, for example, halides,[29] tetrafluoroborate,[30] or bicarbonate/carbonate.[31] Taking into account the well-known fact that the ion effects of anions are stronger than those by cations in the Hofmeister rankings[32] also motivates changing the anions surrounding the cations. There are additionally two important reasons why anions other than hydroxide are convenient; hydroxide reacts detrimentally

Received: August 27, 2013
Revised: December 13, 2013
Published: January 20, 2014

with most ammonium cations, leading to degradation of the cation,[33,34] and hydroxide rapidly reacts with CO_2, establishing equilibrium between hydroxide, bicarbonate, and carbonate. For this reason, there is only a limited set of quality data for hydroxide conductivity in AEMs.[31,35] Therefore, it is essential to study ion transport with various counteranions to understand the properties of these systems and to correlate hydroxide transport with transport of more convenient, less reactive anions.

Previous studies have reported the solvation and transport properties of quaternary ammonium cations.[36] Friedman and co-workers developed a cosphere overlap model, which fits ammonium ion−ion pair interaction to deduce thermodynamic and structural properties of tetraalkyl ammonium halides.[37,38] These models fit an interaction potential derived from statistical mechanics approximations to experimental thermodynamic data. While transport properties cannot be obtained from this model, they do explore thermodynamic properties like excess volume, structure, and heat capacity.

Many studies have either ignored the effects of the counterion on quaternary ammonium cation transport properties or studied ammonium halides, which misses the important issue of the effect of ammonium cations on hydroxide transport. Schmidt, Brown, and Williams studied ^{14}N chemical shifts for various saturated aqueous solutions of ammonia- and ammonium-based compounds and showed that NH_4Br and NH_4Cl have indistinguishable chemical shifts, but the chemical shift of NH_4OH is distinct.[39] They then suggested that TMA with Cl^- or Br^- is distinct from TMA hydroxide based on the ^{14}N NMR shifts, but they were unable to obtain definitive results.[39] Babiaczyk and co-workers performed simulations of quaternary ammonium cations to understand the hydration structure and hydropathicity of these cations.[2] These simulations include a single quaternary ammonium ion; therefore, they considered a low concentration. The interactions between ion pairs, which are expected to be important at finite concentrations, were beyond the scope of their study. Schipper and Kassapidou studied the diffusion of TMA in the presence of various counterions.[40] They found that the measured diffusive transport behavior of TMA appears similar to that of sodium and lithium, but when the counteranion is varied, TMA diffusion is found to change significantly. While the primary goal of their study was to demonstrate that polymethacrylic acid can serve as a simplified model for DNA, they also showed that the diffusion of TMA is significantly affected by the anion. This adds to our motivation to study various quaternary ammonium cations in the presence of different anions. For this study, we have primarily studied TMA, TEA, and benzyltrimethyl ammonium (BMA) (Figure 1), but we have also considered tetrapropyl ammonium (TPA), tetrabutyl ammonium (TBA), and tetrabutyl phosphonium (TBP).

The discussion here is limited to aqueous environments at concentrations between 0.28 and 1.39 M and temperatures between 25 and 80 °C because of solubility and stability concerns with quaternary ammonium cations in the presence of hydroxide at elevated temperatures. Transport properties of cations (quaternary ammonium) and anions like HCO_3^-, CO_3^{2-}, and F^- were measured in this study with PGSTE-NMR, conductivity, and computational techniques. The diffusion of fluoride is particularly useful because it is close in size to hydroxide.[41,42] Notably, this work directly links experiments and simulation, validating the simulation methodology, so that we are able to relate microscopic behavior of the system to macroscopic observables.

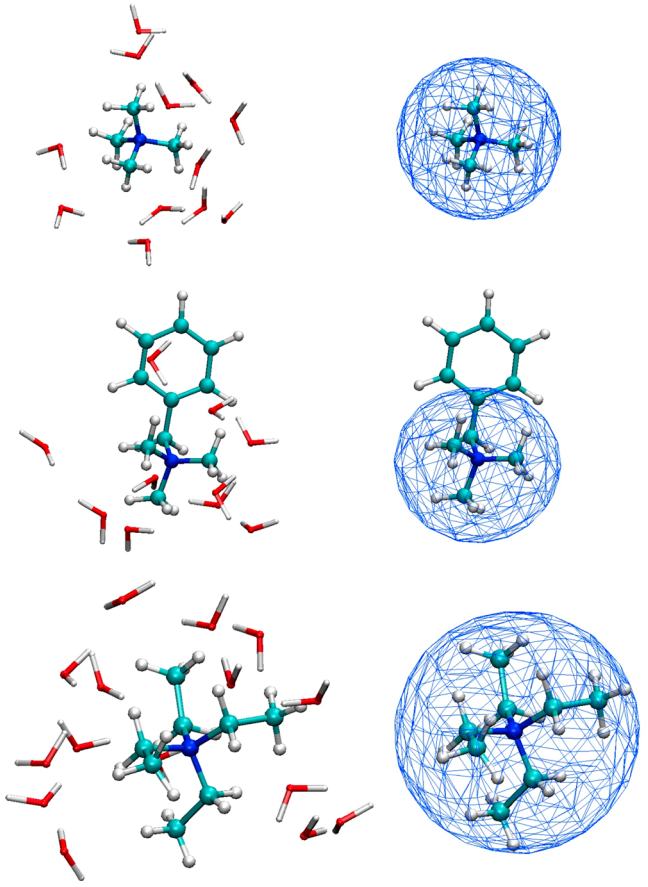

Figure 1. A snapshot of each of the three ammonium cations considered and the electrostatic potential.

2. METHODS

2.1. Experimental Details. *Materials.* TMA hydroxide, TEA hydroxide, TBA hydroxide, BMA hydroxide, and TBP hydroxide were purchased from Sigma Aldrich (U.S.A.) and used as received. ^{13}C-labeled methyl iodide was purchased from Cambridge Isotopes Laboratories (U.S.A.). TMA hydroxide and TBA hydroxide were purchased in solid form, while the remaining ammonium and phosphonium hydroxides were purchased in aqueous solution. Fluoride salts of TMA, TEA, and BMA were purchased from Sigma Aldrich (U.S.A.) and used without purification. The 18 MΩ water was used after degassing with ultrahigh purity (UHP) argon to remove dissolved CO_2.

Synthesis of the ^{13}C-Labeled Tetraalkyl Ammonium Cations. The ^{13}C-labeled methyl iodide was reacted with a trialkyl amine in tetrahydrofuran (THF) at room temperature. The reaction scheme for the synthesis of labeled cations is shown in Scheme 1. A white precipitate was formed by adding ethanol and washed, following a procedure described elsewhere.[43] The resulting salts were dissolved in water and passed through an anion exchange resin column to convert them to the hydroxide form. The resulting solutions were rotavaporized under vacuum to achieve a final concentration of 0.92 M. The concentrated solutions were put in a 5 mm NMR tube to perform the ^{13}C PGSTE NMR diffusion experiments. For this

dx.doi.org/10.1021/jp4085662 | J. Phys. Chem. B 2014, 118, 1363−1372

Scheme 1. Reaction Scheme Employed for the Synthesis of ^{13}C-Labeled Quaternary Ammonium Cations

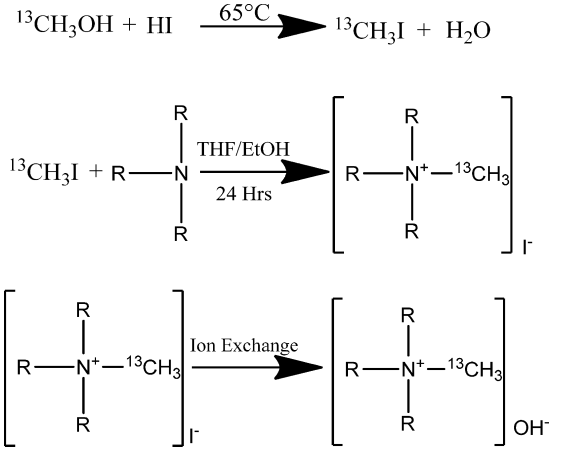

study, the amines used were trimethyl, triethyl, tripropyl, benzyl dimethyl, and tributylamine.

The effect of CO_2 on conductivity was studied for each cation by passing UHP CO_2 through 0.92 M solutions until saturated. After the resulting solutions equilibrated with air, they were used for the conductivity and carbonate/bicarbonate measurements. The carbonate/bicarbonate composition was determined by performing titrations with dilute HCl. The solutions were left in contact with air, and the bicarbonate/carbonate concentration was measured after various intervals of time. After 48 h, the results showed that there was little change in the carbonate/bicarbonate concentration (less than 5%). Thus, we concluded that the carbonate/bicarbonate ratio is stable over the time of our experiments.

Cell Constant Calculations. Conductivity of a solution was calculated by the following equation

$$\kappa = \frac{K}{R} \tag{1}$$

where R is the measured cell resistance and K, the cell constant, was calculated based on the standard conductivity measurements done on a 1 m KCl solution.[44]

Conductivity Experimental Setup. A double-walled water-jacketed electrochemical cell from BASi was used for the conductivity measurements. The electrode system consisted of two gold electrodes and a Ag/AgCl reference electrode. The distance between the two electrodes was maintained constant at 9.3 mm. An inert argon gas blanket was maintained above the solution to avoid contact with atmospheric CO_2. Electrochemical impedance spectroscopy measurements were carried out using a Gamry Potentiostat Reference-600. The measurements were carried out at 25, 45, 65, and 79 °C. Impedance spectra were recorded from 0.2 Hz to 0.1 MHz. The amplitude was 10 mV.

Self-Diffusion Coefficient Measurements. Self-diffusion coefficients of the cations (^{13}C) and anions (^{19}F) were determined with a pulsed field gradient stimulated echo (PGSTE) NMR technique. The diffusion constant, D, was determined by fitting the measured data to the Stejskal–Tanner equation[45]

$$\frac{S}{S_0} = \exp\left[-\gamma^2 G^2 \delta^2 \left(\Delta - \frac{\delta}{3}\right) D\right] \tag{2}$$

where S_0 is the signal amplitude, γ is the gyromagnetic ratio, G is the gradient strength, δ is the length of gradient pulse (1 ms), and Δ is the diffusion time or time between pulses (Figure 2).

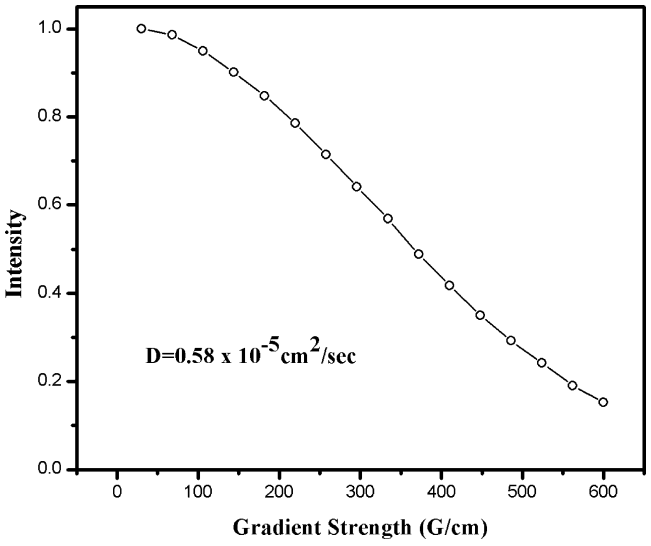

Figure 2. A plot of the experimental points and the line obtained by fitting those points to the Stejskal–Tanner equation. This yields a self-diffusion constant of 0.58 × 10^{-5} cm^2/s for BMA chloride at 25 °C.

The experiments were carried out using a Bruker AVANCEIII NMR spectrometer and 400 MHz (^{1}H frequency) wide bore Magnex magnet. ^{13}C (100.48 MHz) and ^{19}F (376.02 MHz) diffusion measurements were made using a 5 mm Bruker single-axis DIFF60L Z-diffusion probe. The 90° pulse length was on the order of 5 μs. The range of gradient strength was 0–500 G/cm, which was incremented in 16 steps. The maximum value of the gradient was chosen such that the signal decays to 93% of the original value. The Bruker TopSpin software package was used to control the spectrometer and to analyze the data.

When the time between pulses, Δ, is comparable or shorter than some processes in the system, the measured diffusion coefficient is known to depend on Δ (for example, in restricted environments, like membranes or porous media, or in systems with long decorrelation times, like glasses). Because Δ is much longer than any of the relaxation processes typically present in aqueous solutions, the diffusion coefficient is not expected to depend on Δ. To confirm this, we tested three different values of Δ for TPA hydroxide and found similar values for the measured diffusion coefficient (Figure 3). Thus, for all of the measurements described in this work, Δ was chosen to be 20 ms.

2.2. Simulation Details. The ammonium cations and chloride were simulated with molecular dynamics (MD) using the generalized amber force field (GAFF).[46] GAFF has been used previously for the simulation of ammonium ions.[2] Partial charges for the ammonium were determined using the restrained electrostatic potential method as implemented in the Antechamber package.[47,48] Water was modeled using the SPC/Fw potential.[49] All fluoride results shown in this paper employ the model developed by Jensen and Jorgensen,[50] but we also tested the fluoride model developed for use with SPC/E water by Joung and Cheatham[51] and found statistically similar results. The starting MD configurations were prepared by evenly placing 100 ammonium cations in a box and

dx.doi.org/10.1021/jp4085662 | J. Phys. Chem. B 2014, 118, 1363–1372

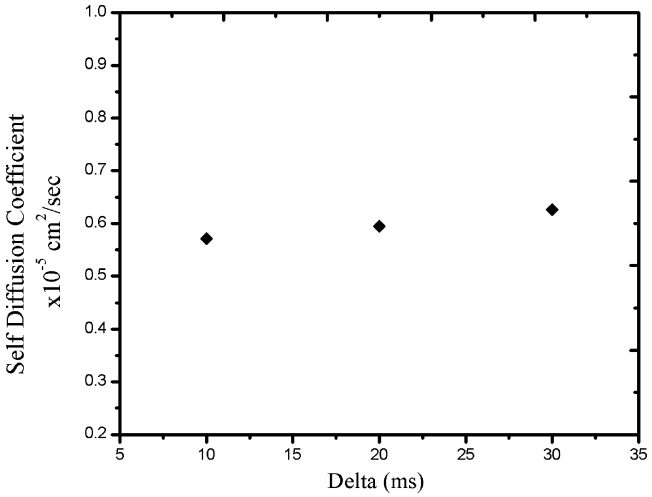

Figure 3. The diffusion coefficient of TPA with a hydroxide counterion as a function of the time between pulses, Δ.

hydrating such that the number of water molecules added was equal to the number of water molecules required to obtain the desired concentration plus one water molecule for each anion. Next, the water molecule closest to a particular ammonium nitrogen atom was replaced with an anion.

Configurations were then energy-minimized for 10 000 steps to remove high-energy interactions between molecules. The minimized structure was annealed at 226.85 °C (500 K) for 500 ps in the constant *NVT* ensemble (constant number of atoms, volume, and temperature). The temperature was then ramped down to 25 °C in 1 ns, saving configurations at 50, 45, 35, and 25 °C. The equilibrium density for each temperature was then obtained by simulating in the constant *NPT* ensemble (constant number of atoms, pressure, and temperature) for 10 ns. The last 5 ns of these simulations were used to determine the average density. The volume was set to achieve the equilibrium density and ran for 2 ns in the constant *NVT* ensemble, and then, starting configurations were obtained from the last 1 ns. Each of these configurations was then simulated for 5 ns in the constant *NVE* ensemble (constant number of atoms, volume, and energy) for the calculation of properties. Simulations were performed using the Amber11 simulation package[52] as implemented for both CPUs and graphics processing units (GPUs).

We use residence times to understand the effect of each ion on short-time dynamics. The residence time is defined in this work as the time that a pair of atoms reside within the first solvation shell, where the first solvation shell is determined from the calculated radial distribution function. We consider cation−anion, cation−water, anion−water, and water−water pairs, where the cation position is taken as the nitrogen atom and the water position is the oxygen atom. In order to account for spurious effects resulting from an atom temporarily moving outside of the cutoff, but not fully entering the bulk, we employ the allowance time approach used by Impey, Madden, and McDonald.[53] A 2 ps allowance time is used to neglect these rattling effects for the calculation of cation−anion, cation−water, and anion−water residence times. Radial distribution functions, mean-squared displacements, and radii of gyration were calculated using Antechamber analysis tools.[47,48]

3. RESULTS

3.1. Conductivity of Quaternary Ammonium Hydroxides. Figure 4a−e shows the temperature and concentration dependence of the experimentally measured conductivity of TMA, BMA, TEA, TBA, and TBP with a hydroxide counterion. The measurements were carried out at 25, 45, 65, and 79 °C.

The highest conductivity is observed with BMA, which is 0.26 S/cm at 65 °C. The alkyl ammonium solutions show a drop in conductivity from TMA to TBA. The one phosphononium-based cation tested results in the lowest conductivities. In general, an Arrhenius dependence on temperature is observed, and a clear trend is seen in the

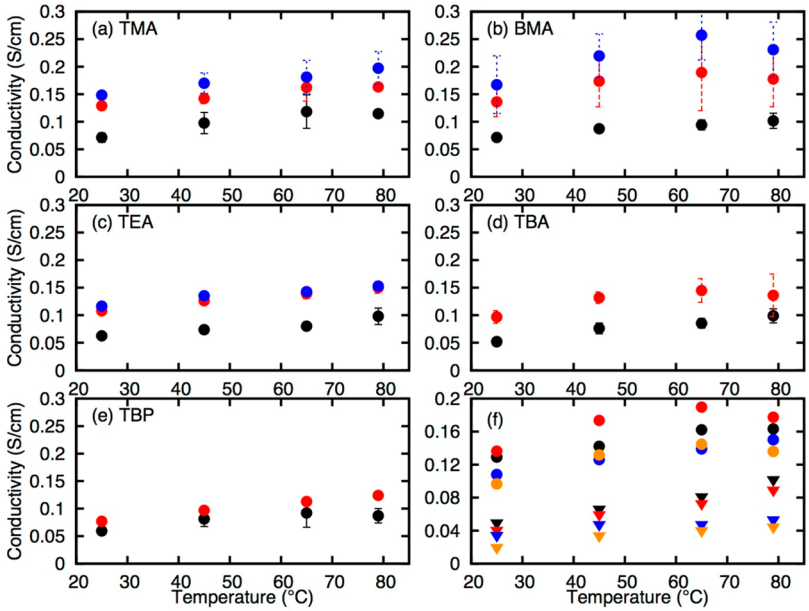

Figure 4. Experimental conductivity of TMA (a), BMA (b), TEA (c), TBA (d), and TBP (e) in hydroxide form as a function of temperature and concentration (0.28 (black), 0.92 (red), and 1.39 M (blue)). The conductivity without CO_2 (circles) and with CO_2 (triangles) is shown for TMA (black), BMA (red), TEA (blue), and TBA (orange) in (f).

dx.doi.org/10.1021/jp4085662 | J. Phys. Chem. B 2014, 118, 1363−1372

activation energy (Table 1). As the alkyl substituent chains are extended, the activation energy increases. BMA, despite having

Table 1. Experimental Activation Energy for Ionic Conductivity for Each Cation with OH^- at 0.92 M

cation	activation energy (kJ/mol)
TMA	3.40 ± 1.24
TEA	5.70 ± 1.26
TBA	8.13 ± 0.77
TBP	10.26 ± 4.56
BMA	5.01 ± 1.50

the largest conductivity, has an activation energy between that of TMA and TEA, and TBP has a significantly larger activation energy than the other cations considered. Conductivity curves are not identical for every cation because of differences in cation size, mass, and solvation. The classical Kohlrausch law describing the independent migration of ions at infinite dilution cannot be reliably applied here because of the nondilute concentration. In these nondilute systems at approximately molar concentrations, there is significant interaction between anions and cations, and these interactions affect ion transport through the solution. As the size of the cation increases, the water molecules in the first solvation shell of the cations become more transient due to weaker electrostatic interactions. To test if long-lived clathrate-like water structures are caging the cations, we plotted the cation diffusion versus the inverse radius of gyration for four cations (Figure 6) and found a linear

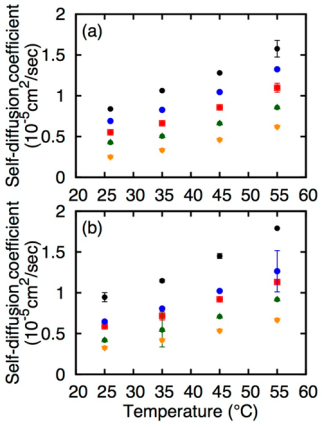

Figure 5. Experimental diffusion coefficients of TMA (black ●), TEA (blue ●), BMA (red ■), TPA (green ●), and TBA (orange ●) in hydroxide form (a) and chloride form (b).

relationship. Therefore, we do not see evidence of long-lived clathrate-like water structures surrounding the cations. The caging is not a uniform effect for the cations considered. The differences arise from the very different electrostatic surfaces, which can be seen on the right in Figure 1. Both TMA and TEA are essentially spherical, but TEA is larger. BMA however has a relatively nonpolar benzyl group extruding from the electrostatic isosurface, making BMA like an amphiphile.

Figure 1 shows snapshots of the solvation structure and electrostatic field of TMA, BMA, and TEA. All three of the cations have an essentially spherical electrostatic field, but the TEA is significantly larger than BMA and TMA. The benzyl ring on BMA is shown to stick outside of the isoelectric surface, while all atoms in TMA and TEA are within the isoelectric

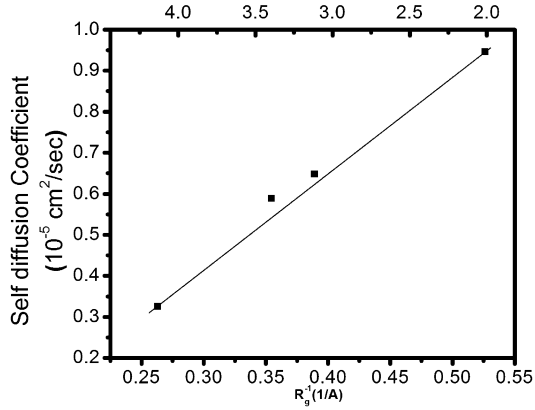

Figure 6. Variation of the self-diffusion coefficient (Table 3) with the radius of gyration for each cation (R_g). The line is intended only to guide the eye.

surface. The representative snapshot of BMA hydration shows that water molecules prefer the methyl groups and not the benzyl group, while hydrating waters are found all around TMA and TEA.

Effect of CO_2 on Conductivity. CO_2 readily reacts with hydroxide to form bicarbonate and in aqueous solution will reach equilibrium with carbonate. To quantify the effect of CO_2 on conductivity, we measured the conductivity of 0.92 M TMA, BMA, TEA, and TBA hydroxide solutions before and after sparging with CO_2 (Figure 4f). There is a significant decrease in the observed conductivity with CO_2. It is interesting to note that the decrease is cation- and anion-dependent. The ratio of conductivity with CO_2 to that without CO_2 is 2.1 ± 0.2, 2.7 ± 0.6, 2.9 ± 0.2, and 3.9 ± 0.8 for TMA, BMA, TEA, and TBA, respectively (averaged over the four temperatures considered). The different effect of CO_2 on each cation results in the highest observed conductivity with CO_2 occurring in the TMA solution, while the highest conductivity without CO_2 was observed in the BMA solution. This conductivity is a combined effect of cation−anion interaction and migration in the solution. Bicarbonate and carbonate ion conductivity is almost one-fourth that of hydroxide, which is one of the causes of this decreased conductivity.

The cause of the drop in conductivity at 79 °C for BMA and TBA hydroxide solutions is unknown. Initially, we thought that this may be due to ion degradation processes, but comparisons of 1D proton NMR measurements before and after the conductivity experiment do not show any signs of degradation.

Self-Diffusion Coefficients. The self-diffusion of various species was determined via PGSTE-NMR and MD simulations. Because we are interested in understanding ionic conductivity in these systems, we consider the self-diffusion coefficients of both cations and anions. Additionally, we are interested in species that permit direct comparison of experiment and theory; therefore we selected ^{13}C-labeled ammonium cations and fluoride (^{19}F) anions.

Figure 5 shows the experimental PGSTE-NMR diffusion coefficient of the ammonium cations with hydroxide and chloride anions. Self-diffusion coefficients were found to strongly correlate with the size of the cation. For the ammonium cations with alkane substituents (all but BMA), cation diffusion is found to scale with the mass of the cation. Despite being heavier, BMA is found to diffuse faster than the TEA, which is attributed to the differences in charge

dx.doi.org/10.1021/jp4085662 | J. Phys. Chem. B 2014, 118, 1363−1372

distribution and the resulting solvation of BMA and TEA (Figure 1). Changing the counterion from hydroxide to chloride weakly influences cation diffusivity. Generally, the self-diffusion coefficients are slightly higher for the chloride counterion than those for the hydroxide, which is likely due to the different solvation of chloride when compared to hydroxide. The experimental values acquired in this study at 0.92 M are compared with the self-diffusion coefficients at infinite dilution, as reported in the literature (Table 3). It is notable that the

Table 2. Comparison of the Activation Energies of Cation Diffusion Estimated from the Simulated and Experimental Results with Cl^- Counter Anions

	simulation (kJ/mol)	experiment (kJ/mol)
TMA	14.9 ± 0.3	17.32 ± 0.95
BMA	15.7 ± 0.2	17.63 ± 0.98
TEA	14. ± 3	17.99 ± 1.01

Table 3. Comparison of the Self-Diffusion Coefficients for Each Cation at 25°C with Cl^- Counter Anions

cation	radius of gyration (s)	D (10^{-5} cm^2/sec) infinite dilution	D (10^{-5} cm^2/sec) 0.92 M
TMA	1.90	1.196[b]	0.945
TEA	2.57	0.868[b]	0.647
BMA	2.82	0.921[b]	0.588
TBA	3.8[a]	0.519[b]	0.325

[a]From Babiaczyk and co-workers.[2] [b]From the CRC Handbook.[61]

slight differences due to the presence of different anions and the large differences due to changing the concentration (Table 3) suggest that ions at 0.92 M do not migrate independently. This indicates that the Nernst–Einstein relationship between conductivities and diffusion coefficients will not be valid. To test this, we calculated the conductivity using the Nernst–Einstein equation[54] from the known cation diffusion coefficient and a hydroxide diffusion[55,56] of 5.30×10^{-5} cm^2/s. For the 0.92 M solution of TMA hydroxide, we estimated the conductivity to be 0.21 S/cm using the Nernst–Einstein equation. This failure of the Nernst–Einstein equation at high concentrations occurs when ion–ion interactions are important. We also used Debye–Hückel–Onsager theory[57] and found that the estimated conductivity is 0.12 S/cm, but Debye–Hückel–Onsager theory lacks information about ion–ion interactions and fails to capture the qualitative ordering of the ionic conductivities. Exact information about these calculations can be found in the Supporting Information.

Figures 7 and 8 compare the diffusion coefficients obtained from PGSTE-NMR experiments and MD simulations. Figure 7 shows the diffusion coefficients of TMA, BMA, and TEA with a chloride counteranion. Both methods indicate that TMA diffuses fastest, followed by BMA and TEA. Figure 8 compares fluoride diffusion in solution with each cation. Fluoride diffusion is found, independent of method, to be fastest in the TMA solution and to be similar in the BMA and TEA solutions. Figure 9 shows a comparison of BMA self-diffusion coefficients with chloride, fluoride, and hydroxide.

We also attempted to measure the diffusion of ^{13}C-labeled carbonate and bicarbonate using PGSTE-NMR. When the carbon atoms in carbonate or bicarbonate are present individually, they show the expected chemical shifts, but when they coexist in a solution, they appear as a single NMR peak. Thus, we were unable to discern the individual self-diffusion coefficients of carbonate and bicarbonate.

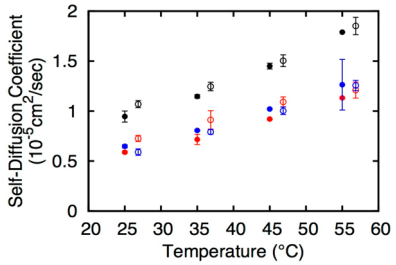

Figure 7. A comparison of the experimental (●) and simulated (○) self-diffusion coefficients for TMA (black), BMA (red), and TEA (blue) cations with Cl^- counterions.

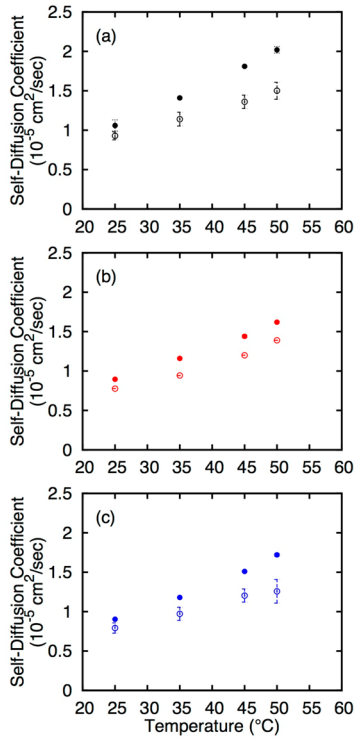

Figure 8. Experimental (●) and simulated (○) self-diffusion coefficients of fluoride in the presence of R_4N^+, where (a) is F^- diffusion with a TMA counterion, (b) is F^-diffusion with a BMA counterion, and (c) is F^- diffusion with a TEA counterion. The simulated fluoride diffusion constants are 10–25% smaller than those from experiment.

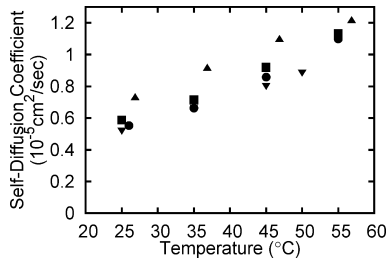

Figure 9. A comparison of the ^{13}C BMA self-diffusion coefficient values obtained with each method and counteranion. Using PGSTE-NMR, we determined the BMA self-diffusion coefficient with chloride (■) and hydroxide (●), and with MD, we determined the BMA self-diffusion coefficient with chloride (▲) and fluoride (▼).

dx.doi.org/10.1021/jp4085662 | J. Phys. Chem. B 2014, 118, 1363–1372

We approximated the activation energy for diffusion of each cation by fitting cation diffusion to the Arrhenius equation (Table 2). The activation energy has minimal dependence on the cation. The simulated and experimental activation energies are in the same range, but the large error makes the trends difficult to compare.

The diffusion coefficients from experiment and simulation are generally in good agreement. For the cation diffusion coefficients, the TMA experimental results agree very well with the simulations. For both experiment and simulation, BMA and TEA are similar and within the error of each other at many temperatures, but experiment does indicate that BMA is faster, while simulation indicates that TEA is faster. If this difference is real, and not just an artifact of the error in the data, it can be attributed to using a generalized force field for the cations, instead of one specially designed for these solutions and the slightly different mass of ^{13}C-labeled TEA, which has one ethyl group replaced with a methyl group. For the anion diffusion coefficients, the simulation results are found to be 10−25% smaller than experiment. To test if this discrepancy results from the Jensen and Jorgensen fluoride model being poorly suited for simulation with these cations, we also tested a model parametrized by Joung and Cheatham for use in biomolecular simulations.[51] The Joung and Cheatham model behaved similarly (not shown) to the Jensen and Jorgensen model. Because the discrepancy occurs in multiple models, we expect that a new fluoride model would need to be developed specifically for this type of system. However, the general level of agreement between experiment and theory validates the GAFF force field and permits the screening of cations without the burden of first parametrizing a force field.

Residence Time. As discussed previously, the Nernst−Einstein equation does not apply to these systems because of interactions between the ions. We therefore used residence time as a way to understand ion−ion and ion−water interactions. The average residence times calculated from MD simulations are shown in Figure 10. In Figure 10a, the anion−water residence time is seen to very weakly depend on the cation present. This indicates that the cation has only a weak effect on the solvation of the anion. Figure 10b shows the residence time for the cation−anion pair. TMA has the longest-lived ion pair, while BMA and TEA are very similar. Figure 10c shows the cation−water residence time. BMA results in the shortest-lived water−cation pair, followed by TMA and TEA, showing that water molecules remain around TEA about 1 ps longer than around BMA. This is also reflected in the water−water residence times shown in Figure 10d, where water−water residence times are longest in the TEA solution. This provides some rationale for the discrepancy between the observed conductivities and diffusivities. Because the pairing of these ions with the water molecules around them is different, we expect them to be transported through solution differently.

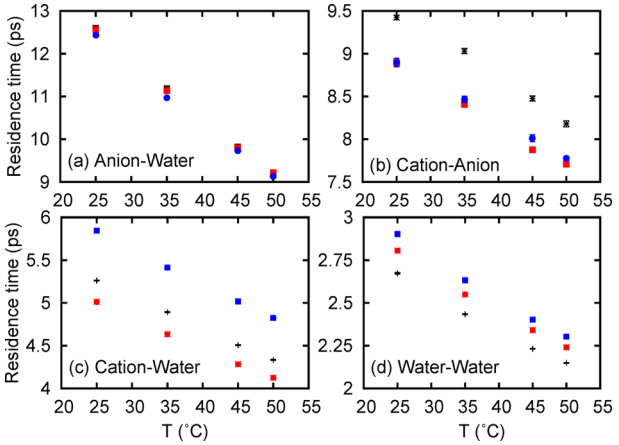

Figure 10. The calculated residence times of various important pairs in the solutions with TMA (black), BMA (red), and TEA (blue).

Structure and Solvation of Ammonium Cations. The mean radius of gyration was calculated from the simulations to be 1.90, 2.57, and 2.82 Å for TMA, TEA, and BMA, respectively. These values were determined at 25 °C, but the radius of gyration is constant across the temperatures considered here. These values are in good agreement with 1.93 and 2.53 Å for TMA and TEA, as determined by Babiaczyk and co-workers.[2]

Additionally a number of radial distribution functions and integrated coordination numbers were calculated. Figure 11a shows the oxygen in water to nitrogen in ammonium radial distribution functions and coordination numbers. TMA has a tall first peak, with small peaks farther out. The BMA radial distribution function is similar, with slightly reduced magnitude in the first peak. It appears that the benzyl group in BMA serves to exclude water from approaching in that region but generally does not affect solvation around the methyl groups. TEA solvation is distinctly different than TMA and BMA though. Figure 11b shows the fluoride−nitrogen radial distribution functions and coordination numbers. As for nitrogen−water, TMA is found to have the largest magnitude first peak, and BMA is found to have similar but reduced structure. Figure 11c and d shows fluoride−fluoride radial distribution functions and coordination numbers. Figure 11c shows that the cations have minimal effect on the solvation of fluoride, which is in line with Figure 10a. Figure 11d shows each temperature considered for BMA. Temperature has the expected effect, but it is minimal over this small temperature range.

There are other examples in the literature where aqueous solution studies have been used to help understand materials for fuel cells. Pivovar and co-workers have studied quaternary ammonium cations in the presence of hydroxide experimentally[58,59] and by DFT calculations.[33] Schuster and co-workers have studied ion transport in similar systems containing an acidic group connected to a long chain to mimic their nature in proton exchange membrane fuel cells.[60] The direct connection of experiment and molecular theory validates the results and provides molecular insight into the macroscopic observations. For example, there is a wide range of cations proposed for use in anion exchange fuel cells, but often, initial characterization occurs in membranes where the backbone membrane material, morphology and membrane preparation methodology, counterions, and temperature can all have unknown effects. The methodology in this paper cannot replace testing in more realistic environments, but it does permit a first pass scheme to understand the relative effects of different cations on local water structure and anion transport. We have shown how short- and long-time dynamics appear to support the use of BMA over the other cations tested. The fluoride ion diffusion measurement approach can be further extended to study membrane morphology and ion transport in AEMs without the caustic effects of hydroxide anions.

dx.doi.org/10.1021/jp4085662 | J. Phys. Chem. B 2014, 118, 1363−1372

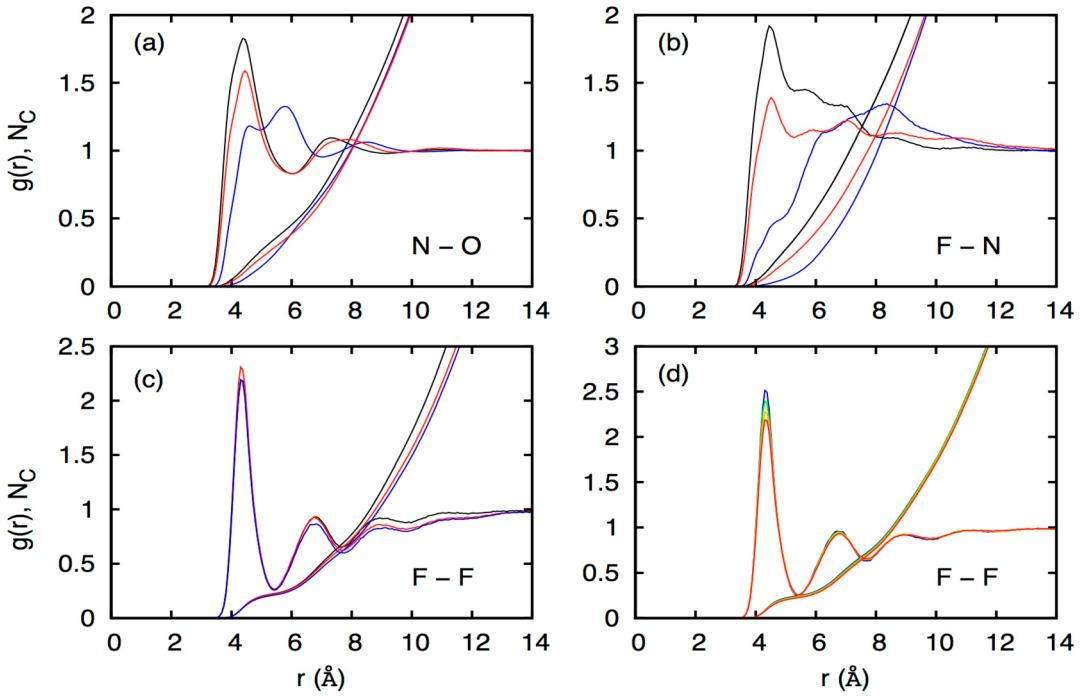

Figure 11. The effect of the cation on the atomic solvation structure is shown by comparing radial distribution functions ($g(r)$) and integrated coordination numbers (N_C). (a–c) The effects of TMA (black), BMA (red), and TEA (blue) are compared for nitrogen and oxygen atoms (a), fluoride and nitrogen atoms (b) and fluoride and fluoride ions (c). (d) The $g(r)$ and N_C are shown for fluoride self-coordination in the presence of TMA at 25 (blue), 35 (green), 45 (orange), and 50 °C (red), demonstrating the weak temperature dependence.

4. CONCLUSIONS

In this work, we have investigated the transport and solvation of quaternary ammonium cations and various counteranions in aqueous solutions experimentally and by simulation. The ionic conductivity was measured with and without CO_2. We demonstrated that CO_2 depresses conductivity by more than 50%, but the specific trends are not transferable between different cations. We showed that the Nernst–Einstein equation poorly relates the conductivity in these solutions to experimental self-diffusion coefficients, which suggests that diffusion coefficients measurements are insufficient to understand the observed conductivity. The Nernst–Einstein and Debye–Hückel–Onsager theories of conductivity were developed for dilute systems; thus, they incorrectly estimated ionic conductivity when applied to these concentrated solutions. To solve this problem, we paired diffusion measurements with residence times to understand the interplay between short-time and long-time dynamics with ionic conductivity. Of the cations studied, solutions with BMA are the most conductive. We were able to use the simulated ion–water residence times to show that BMA and water molecules form the shortest-lived contact pair. This helps to explain the increased conductivity of the BMA cation compared to the other cations studied here, suggesting that BMA is better suited for AEMs compared to TMA or TEA.

■ ASSOCIATED CONTENT

Supporting Information

Calculations of the conductivity using Nernst–Einstein and Debye–Hückel–Onsager equations are provided. This material is available free of charge via the Internet at http://pubs.acs.org.

■ AUTHOR INFORMATION

Corresponding Authors

*E-mail: gavoth@uchicago.edu (G.A.V.).
*E-mail: aherring@mines.edu (A.M.H.).

Author Contributions

⊥H.N.S. and G.E.L. contributed equally.

Notes

The authors declare no competing financial interest.

■ ACKNOWLEDGMENTS

We thank the Army Research Office for funding this Multidisciplinary University Research Initiative under Contract W911NF-10-1-0520 and the Colorado School of Mines NMR facility, funded by National Science Foundation under the Grant CHE-0923537.

■ REFERENCES

(1) MacKinnon, R.; Yellen, G. Mutations Affecting TEA Blockade and Ion Permeation in Voltage-Activated K+ Channels. *Science* **1990**, *250*, 276–279.

(2) Babiaczyk, W. I.; Bonella, S.; Guidoni, L.; Ciccotti, G. Hydration Structure of the Quaternary Ammonium Cations. *J. Phys. Chem. B* **2010**, *114*, 15018–15028.

(3) Lan, C. J.; Lee, C. Y.; Chin, T. S. Tetra-Alkyl Ammonium Hydroxides as Inhibitors of Zn Dendrite in Zn-Based Secondary Batteries. *Electrochim. Acta* **2007**, *52*, 5407–5416.

(4) Couture, G.; Alaaeddine, A.; Boschet, F.; Ameduri, B. Polymeric Materials as Anion-Exchange Membranes for Alkaline Fuel Cells. *Prog. Polym. Sci.* **2011**, *36*, 1521–1557.

(5) Merle, G.; Wessling, M.; Nijmeijer, K. Anion Exchange Membranes for Alkaline Fuel Cells: A Review. *J. Membr. Sci.* **2011**, *377*, 1–35.

(6) Kawai, K.; Kaneko, K.; Yonezawa, T. Hydrophilic Quaternary Ammonium Type Ionic Liquids. Systematic Study of the Relationship

among Molecular Structures, Osmotic Pressures, and Water-Solubility. *Langmuir* **2011**, *27*, 7353−7356.
(7) Samakande, A.; Hartmann, P. C.; Sanderson, R. D. Synthesis and Characterization of New Cationic Quaternary Ammonium Polymerizable Surfactants. *J. Colloid Interface Sci.* **2006**, *296*, 316−323.
(8) Starks, C. M. Heterogeneous Reactions Involving Anion Transfer by Quaternary Ammonium and Phosphonium Salts. *J. Am. Chem. Soc.* **1971**, *93*, 195−199.
(9) Leng, Y. J.; Chen, G.; Mendoza, A. J.; Tighe, T. B.; Hickner, M. A.; Wang, C. Y. Solid-State Water Electrolysis with an Alkaline Membrane. *J. Am. Chem. Soc.* **2012**, *134*, 9054−9057.
(10) Faraj, M.; Boccia, M.; Miller, H.; Martini, F.; Borsacchi, S.; Geppi, M.; Pucci, A. New LDPE Based Anion-Exchange Membranes for Alkaline Solid Polymeric Electrolyte Water Electrolysis. *Int. J. Hydrogen Energy* **2012**, *37*, 14992−15002.
(11) Brand, H. V.; Curtiss, L. A.; Iton, L. E.; Trouw, F. R.; Brun, T. O. Theoretical and Inelastic Neutron-Scattering Studies of Tetraethylammonium Cation as a Molecular-Sieve Template. *J. Phys. Chem.* **1994**, *98*, 1293−1301.
(12) Coletta, F.; Ferrarini, A.; Gottardi, F.; Nordio, P. L. NMR Relaxation in Long-Chain Quaternary Ammonium-Ions — The Role of Torsional Flexibility. *Chem. Phys.* **1995**, *192*, 19−24.
(13) Wait, E.; Powell, H. M. The Crystal and Molecular Structure of Tetraethylammonium Iodide. *J. Chem. Soc.* **1958**, 1872−1875.
(14) Nagano, Y.; Mizuno, H.; Sakiyama, M.; Fujiwara, T.; Kondo, Y. Hydration Enthalpy of Tetra-Normal-Butylammonium Ion. *J. Phys. Chem.* **1991**, *95*, 2536−2540.
(15) Paddison, S. J.; Kreuer, K.-D.; Maier, J. About the Choice of the Protogenic Group in Polymer Electrolyte Membranes: Ab Initio Modelling of Sulfonic Acid, Phosphonic Acid, and Imidazole Functionalized Alkanes. *Phys. Chem. Chem. Phys.* **2006**, *8*, 4530−4542.
(16) Kreuer, K.-D.; Paddison, S. J.; Spohr, E.; Schuster, M. Transport in Proton Conductors for Fuel-Cell Applications: Simulations, Elementary Reactions, and Phenomenology. *Chem. Rev.* **2004**, *104*, 4637−4678.
(17) Paddison, S. J.; R. Pratt, L.; Zawodzinski, T.; Reagor, D. W. Molecular Modeling of Trifluoromethanesulfonic Acid for Solvation Theory. *Fluid Phase Equilib.* **1998**, *150*−*151*, 235−243.
(18) Koga, Y.; Sebe, F.; Nishikawa, K. Effects of Tetramethyl- and Tetraethylammonium Chloride on H_2O: Calorimetric and Near-Infrared Spectroscopic Study. *J. Phys. Chem. B* **2012**, *117*, 877−883.
(19) Finney, J. L.; Soper, A. K. Solvent Structure and Perturbations in Solutions of Chemical and Biological Importance. *Chem. Soc. Rev.* **1994**, *23*, 1−10.
(20) Stangret, J.; Gampe, T. Hydration Sphere of Tetrabutylammonium Cation. FTIR Studies of HDO Spectra. *J. Phys. Chem. B* **1999**, *103*, 3778−3783.
(21) Turner, J. Z.; Soper, A. K.; Finney, J. L. Ionic versus Apolar Behavior of the Tetramethylammonium Ion in Water. *J. Chem. Phys.* **1995**, *102*, 5438−5443.
(22) Turner, J.; Soper, A. K. The Effect of Apolar Solutes on Water-Structure — Alcohols and Tetraalkylammonium Ions. *J. Chem. Phys.* **1994**, *101*, 6116−6125.
(23) Varcoe, J. R.; Slade, R. C. T. Prospects for Alkaline Anion-Exchange Membranes in Low Temperature Fuel Cells. *Fuel Cells* **2005**, *5*, 187−200.
(24) Hibbs, M. R.; Fujimoto, C. H.; Cornelius, C. J. Synthesis and Characterization of Poly(phenylene)-Based Anion Exchange Membranes for Alkaline Fuel Cells. *Macromolecules* **2009**, *42*, 8316−8321.
(25) Zhang, Y. M.; Fang, J.; Wu, Y. B.; Xu, H. K.; Chi, X. J.; Li, W.; Yang, Y. X.; Yan, G.; Zhuang, Y. Z. Novel Fluoropolymer Anion Exchange Membranes for Alkaline Direct Methanol Fuel Cells. *J. Colloid Interface Sci.* **2012**, *381*, 59−66.
(26) Gu, S.; Cai, R.; Luo, T.; Chen, Z. W.; Sun, M. W.; Liu, Y.; He, G. H.; Yan, Y. S. A Soluble and Highly Conductive Ionomer for High-Performance Hydroxide Exchange Membrane Fuel Cells. *Angew. Chem., Int. Ed.* **2009**, *48*, 6499−6502.
(27) Jung, M. S. J.; Arges, C. G.; Ramani, V. A Perfluorinated Anion Exchange Membrane with a 1,4-Dimethylpiperazinium Cation. *J. Mater. Chem.* **2011**, *21*, 6158−6160.
(28) Gu, S.; Cai, R.; Yan, Y. Self-Crosslinking for Dimensionally Stable and Solvent-Resistant Quaternary Phosphonium Based Hydroxide Exchange Membranes. *Chem. Commun.* **2011**, *47*, 2856−2858.
(29) Arges, C. G.; Parrondo, J.; Johnson, G.; Nadhan, A.; Ramani, V. Assessing the Influence of Different Cation Chemistries on Ionic Conductivity and Alkaline Stability of Anion Exchange Membranes. *J. Mater. Chem.* **2012**, *22*, 3733−3744.
(30) Tsai, T.-H.; Maes, A. M.; Vandiver, M. A.; Versek, C.; Seifert, S.; Tuominen, M.; Liberatore, M. W.; Herring, A. M.; Coughlin, E. B. Synthesis and Structure−Conductivity Relationship of Polystyrene-Block-Poly(vinyl benzyl trimethylammonium) for Alkaline Anion Exchange Membrane Fuel Cells. *J. Polym. Sci., Part B: Polym. Phys.* **2013**, *51*, 1751−1760.
(31) Yan, J.; Hickner, M. A. Anion Exchange Membranes by Bromination of Benzylmethyl-Containing Poly(sulfone)s. *Macromolecules* **2010**, *43*, 2349−2356.
(32) Koga, Y. *Solution Thermodynamics and its Application to Aqueous Solutions: A Differential Approach*, 1st ed.; Elsevier Science: Amsterdam, The Netherlands, 2007.
(33) Long, H.; Kim, K.; Pivovar, B. S. Hydroxide Degradation Pathways for Substituted Trimethylammonium Cations: A DFT Study. *J. Phys. Chem. C* **2012**, *116*, 9419−9426.
(34) Chempath, S.; Einsla, B. R.; Pratt, L. R.; Macomber, C. S.; Boncella, J. M.; Rau, J. A.; Pivovar, B. S. Mechanism of Tetraalkylammonium Headgroup Degradation in Alkaline Fuel Cell Membranes. *J. Phys. Chem. C* **2008**, *112*, 3179−3182.
(35) Janarthanan, R.; Horan, J. L.; Caire, B. R.; Ziegler, Z. C.; Yang, Y.; Zuo, X.; Liberatore, M. W.; Hibbs, M. R.; Herring, A. M. Understanding Anion Transport in an Aminated Trimethyl Polyphenylene with High Anionic Conductivity. *J. Polym. Sci., Part B: Polym. Phys.* **2013**, *51*, 1743−1750.
(36) Luzhkov, V. B.; Osterberg, F.; Acharya, P.; Chattopadhyaya, J.; Aqvist, J. Computational and NMR Study of Quaternary Ammonium Ion Conformations in Solution. *Phys. Chem. Chem. Phys.* **2002**, *4*, 4640−4647.
(37) Ramanathan, P. S.; Krishnan, C. V.; Friedman, H. Models Having the Thermodynamic Properties of Aqueous Solutions of Tetraalkylammonium Halides. *J. Solution Chem.* **1972**, *1*, 237−262.
(38) Streng, W. H.; Wen, W.-Y. Calculation of Gurney Parameters for Aqueous Tetraalkylammonium Halides Based on Friedman's Cosphere-Overlap Model. *J. Solution Chem.* **1974**, *3*, 866−880.
(39) Schmidt, B. M.; Carlton Brown, L.; Williams, D. Chemical Shifts of N14 in the NMR Spectra of Ammonia and Related Compounds. *J. Mol. Spectrosc.* **1958**, *2*, 539−550.
(40) Schipper, F. J. M.; Kassapidou, K.; Leyte, J. C. Polyelectrolyte Effects on Counterion Self-Diffusion. *J. Phys.: Condens. Matter* **1996**, *8*, 9301−9308.
(41) Volkov, V. I.; Popkov, Y. M.; Timashev, S. F.; Bessarabov, D. G.; Sanderson, R. D.; Twardowski, Z. Self-Diffusion of Water and Fluorine Ions in Anion-Exchange Polymeric Materials (Membranes and Resin) as Determined by Pulsed-Field Gradient Nuclear Magnetic Resonance Spectroscopy. *J. Membr. Sci.* **2000**, *180*, 1−13.
(42) Sodaye, S.; Suresh, G.; Pandey, A. K.; Goswami, A. Determination and Theoretical Evaluation of Selectivity Coefficients of Monovalent Anions in Anion-Exchange Polymer Inclusion Membrane. *J. Membr. Sci.* **2007**, *295*, 108−113.
(43) Guijarro, D.; Martinez, P. J.; Najera, C.; Yus, M. Benzyllithium from Methylated Benzylamine and Its Ammonium Salt via Naphthalene-Catalyzed Carbon−Nitrogen Bond Reductive Cleavage. *Arkivoc* **2004**, 5−13.
(44) Pratt, K. W.; Koch, W. F.; Wu, Y. C.; Berezansky, P. A. Molality-Based Primary Standards of Electrolytic Conductivity — (IUPAC Technical Report). *Pure Appl. Chem.* **2001**, *73*, 1783−1793.

(45) Stejskal, E. O.; Tanner, J. E. Spin Diffusion Measurements: Spin Echoes in the Presence of a Time-Dependent Field Gradient. *J. Chem. Phys.* **1965**, *42*, 288−292.
(46) Wang, J.; Wolf, R. M.; Caldwell, J. W.; Kollman, P. A.; Case, D. A. Development and Testing of a General Amber Force Field. *J. Comput. Chem.* **2004**, *25*, 1157−1174.
(47) Wang, J. M.; Wang, W.; Kollman, P. A.; Case, D. A. Automatic Atom Type and Bond Type Perception in Molecular Mechanical Calculations. *J. Mol. Graphics Modell.* **2006**, *25*, 247−260.
(48) Wang, J. M.; Wolf, R. M.; Caldwell, J. W.; Kollman, P. A.; Case, D. A. Development and Testing of a General Amber Force Field. *J. Comput. Chem.* **2004**, *25*, 1157−1174.
(49) Wu, Y. J.; Tepper, H. L.; Voth, G. A. Flexible Simple Point-Charge Water Model with Improved Liquid-State Properties. *J. Chem. Phys.* **2006**, *124*, 024503.
(50) Jensen, K. P.; Jorgensen, W. L. Halide, Ammonium, and Alkali Metal Ion Parameters for Modeling Aqueous Solutions. *J. Chem. Theory Comput.* **2006**, *2*, 1499−1509.
(51) Joung, I. S.; Cheatham, T. E. Determination of Alkali and Halide Monovalent Ion Parameters for Use in Explicitly Solvated Biomolecular Simulations. *J. Phys. Chem. B* **2008**, *112*, 9020−9041.
(52) Case, D. A.; Cheatham, T. E.; Darden, T.; Gohlke, H.; Luo, R.; Merz, K. M.; Onufriev, A.; Simmerling, C.; Wang, B.; Woods, R. J. The Amber Biomolecular Simulation Programs. *J. Comput. Chem.* **2005**, *26*, 1668−1688.
(53) Impey, R. W.; Madden, P. A.; McDonald, I. R. Hydration and Mobility of Ions in Solution. *J. Phys. Chem.* **1983**, *87*, 5071−5083.
(54) Borucka, A. Z.; Bockris, J. O. M.; Kitchener, J. A. Test of the Applicability of the Nernst−Einstein Equation to Self-Diffusion and Conduction of Ions in Molten Sodium Chloride. *J. Chem. Phys.* **1956**, *24*, 1282−1282.
(55) Lee, S. H.; Rasaiah, J. C. Proton Transfer and the Mobilities of the H+ and OH− Ions from Studies of a Dissociating Model for Water. *J. Chem. Phys.* **2011**, *135*, 124505−124510.
(56) Light, T. S.; Licht, S.; Bevilacqua, A. C.; Morash, K. R. The Fundamental Conductivity and Resistivity of Water. *Electrochem. Solid-State Lett.* **2005**, *8*, E16−E19.
(57) Hamann, C. H.; Andrew, H.; Vielstich, W. *Electrochemistry*; John Wiley & Sons: New York, 1998.
(58) Edson, J. B.; Macomber, C. S.; Pivovar, B. S.; Boncella, J. M. Hydroxide Based Decomposition Pathways of Alkyltrimethylammonium Cations. *J. Membr. Sci.* **2012**, *399−400*, 49−59.
(59) Macomber, C. S.; Boncella, J. M.; Pivovar, B. S.; Rau, J. A. Decomposition Pathways of an Alkaline Fuel Cell Membrane Material Component via Evolved Gas Analysis. *J. Therm. Anal. Calorim.* **2008**, *93*, 225−229.
(60) Schuster, M.; Rager, T.; Noda, A.; Kreuer, K. D.; Maier, J. About the Choice of the Protogenic Group in PEM Separator Materials for Intermediate Temperature, Low Humidity Operation: A Critical Comparison of Sulfonic Acid, Phosphonic Acid and Imidazole Functionalized Model Compounds. *Fuel Cells* **2005**, *5*, 355−365.
(61) Haynes, W. M. *CRC Handbook of Chemistry and Physics*, 93rd ed.; Taylor & Francis: London, 2012.